THE JOURNAL OF PHYSICAL CHEMISTRY B LETTERS

2006, *110,* 14050−14054
Published on Web 07/01/2006

Size-Manipulable Synthesis of Single-Crystalline $BaMnO_3$ and $BaTi_{1/2}Mn_{1/2}O_3$ Nanorods/Nanowires

C. G. Hu,[†,‡] H. Liu,[†,§] C. S. Lao,[†] L. Y. Zhang,[||] D. Davidovic,[||] and Z. L. Wang*[,†]

School of Materials Science and Engineering, Georgia Institute of Technology, Atlanta, Georgia 30332, Department of Applied Physics, Chongqing University, Chongqing 400044, China, State Key Laboratory of Crystal Materials, Shandong University, Jinan 250100, China, and School of Physics, Georgia Institute of Technology, Atlanta, Georgia 30332

Received: June 4, 2006; In Final Form: June 19, 2006

We report a size-manipulable synthesis of single-crystalline nanorods/nanowires of barium manganite ($BaMnO_3$) and barium titanium manganite ($BaTi_{1/2}Mn_{1/2}O_3$) by using the composite-hydroxide-mediated approach. The synthesis cleanly yields nanorods with a hexagonal perovskite structure. Typical nanorods have widths ranging between 50 and 100 nm, and the lengths can be easily controlled by time and temperature or by adding a small amount of water during the synthesis process. Resistance measurement shows that a phase transition happened at 58 K on $BaMnO_3$. The photoluminescence spectrum of $BaTi_{1/2}Mn_{1/2}O_3$ presents two emission peaks at wavelengths of 465 and 593 nm, corresponding to blue and green fluorescence. The ability to synthesize nanorod manganites of a desired length should enable detailed investigations of the size-dependent evolution of magnetism, magnetoresistance, nanoscale phase separation, and realization of a nanodevice of magnetic sensors.

1. Introduction

Nanocrystalline materials typically exhibit physical and chemical properties that are distinct from their bulk counterparts.[1−3] The properties of manganites are expected to depend on material size due to both the nanoscale phase in homogeneity inherent to bulk materials and additional surface effects.[4−11] Previous investigations on thin-film manganite samples have shown that their properties depend sensitively on the film thickness, leading to surface-induced phase separation[4−6] and strain-dependent metal−insulator transitions (MITs).[8] Although advances have been made in the preparation of nano- and microcrystalline oxides including manganites,[12−20] detailed physical investigations of nanocrystalline manganites have not been possible due to the lack of reliable methods to prepare well-isolated manganite nanocrystals with variable shape and size, especially in one dimension. One-dimensional nano-manganites play a key role in the realization of highly sensitive magnetic nanosensors, because they can be easily fabricated into field-effect transistors (FETs) used in current−voltage or resistance measurements under a magnetic field.

This paper is focused on synthesis methods for the manganites, particularly with the aim of developing low-temperature routes that might provide access to variable shape and size. Like most complex metal oxides, the solids have most commonly been prepared using the high-temperature (more than 1000 °C) ceramic method of solid-state chemistry, involving the grinding and firing of oxide precursors. Besides the difficulties in achieving sample homogeneity for multinary oxides, control of oxygen content in mixed-valent systems requires some synthetic skill when the ceramic method is used, and often several steps, involving a controlled gas atmosphere to optimize the oxidation state of manganese, are necessary.[21] Other synthesis methods that have been adopted for the manganites include the sol−gel[22,23] and coprecipitation[24,25] methods, but these typically involve a final firing or annealing step at high temperature and thus cannot be considered to be true low-temperature synthesis methods. The size of a single manganite is usually in micrometers, and the shape is often ill-shaped by the methods mentioned above. Recently, a hydrothermal route to the manganites has been reported,[20,26−29] but the size of the manganities, commonly particles, are not uniform and range from tens to hundreds nanometers and the size and shape can hardly be controlled by the hydrothermal method. Here, we report a shape- and size-manipulable approach for the synthesis of barium manganite ($BaMnO_3$) and barium titanium manganite ($BaTi_{1/2}Mn_{1/2}O_3$) nanostructures. The method is based on a reaction between a metallic salt and a metallic oxide in a solution of molten mixed potassium hydroxide and sodium hydroxide at ∼200 °C and normal atmosphere without using organic dispersant or capping agent.[30] This methodology provides a one-step, convenient, low-cost, nontoxic, mass-production route for the synthesis of manganite nanostructures in a variety of sizes.

2. Experimental Section

The synthesis of the $BaMnO_3$ follows the following steps.[30] (1) An amount of 20 g of mixed hydroxides (MHDs) (NaOH/

* Corresponding author. E-mail: zhong.wang@mse.gatech.edu.
[†] School of Materials Science and Engineering, Georgia Institute of Technology.
[‡] Chongqing University.
[§] Shandong University.
[||] School of Physics, Georgia Institute of Technology.

10.1021/jp063459+ CCC: $33.50

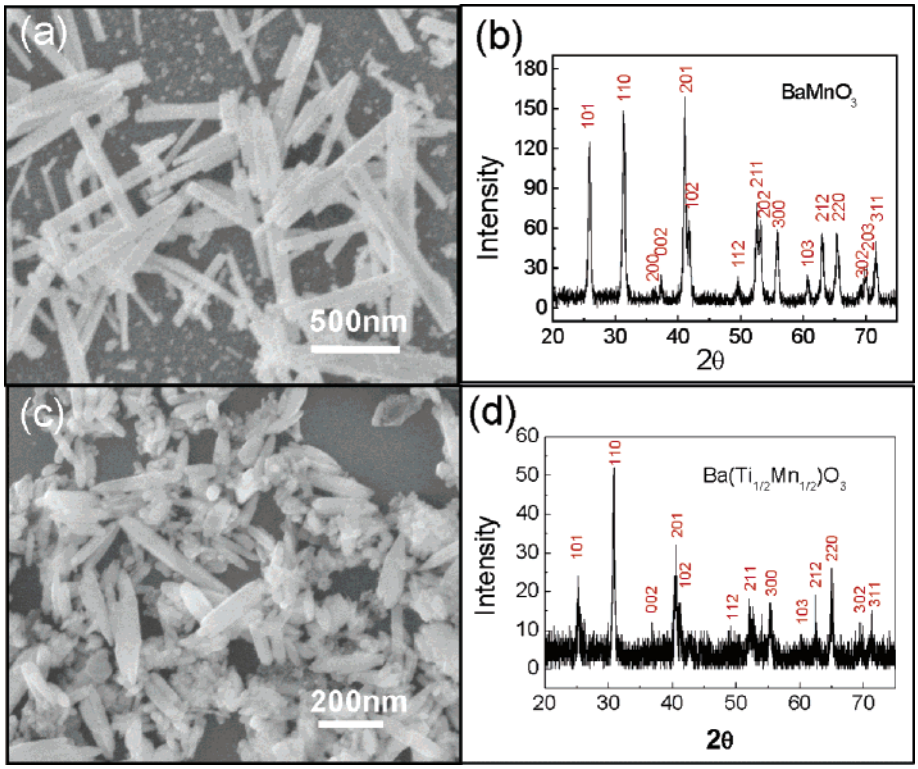

Figure 1. Perovskite (a and b) $BaMnO_3$ and (c and d) $BaTi_{0.5}Mn_{0.5}O_3$ nanorods synthesized by the composite-hydroxide-mediated approach: (a) SEM image and (b) XRD pattern of the $BaMnO_3$ nanorods at 170 °C for 72 h; (c) SEM image and (d) XRD pattern of the $BaTi_{0.5}Mn_{0.5}O_3$ nanorods at 200 °C for 48 h.

KOH = 51.5:48.5) was placed in a 25 mL covered Teflon vessel. (2) A mixture of anhydrous $BaCl_2$ and MnO_2 at 0.5 mmol each was used as the raw material for reaction. (3) The raw material was placed on the top of the hydroxide in the vessel. The vessel was put in a furnace, which was preheated to 170−200 °C. (4) After the hydroxides were totally molten, the molten hydroxide solution was stirred by a platinum bar or by shaking the covered vessel to ensure uniformly mixed reactants. (5) After reacting for 24−120 h, the vessel was taken out and cooled to room temperature. The solid product was dissolved by deionized water. The product was filtered and washed by first deionized water and then hot water to remove hydroxide on the surface of the particles. The synthesized product was received. For the synthesis of the $BaTi_{1/2}Mn_{1/2}O_3$, all of the synthesis procedures are the same as those stated above except replacing the raw materials in step 2. A mixture of $BaCl_2$, MnO_2, and TiO_2 at 0.422, 0.221, and 0.221 mmol, respectively, was used as the raw material for the synthesis of the $BaTi_{1/2}Mn_{1/2}O_3$.

Scanning electron microscopy (FE-SEM) (field emission LEO1530) and transmission electron microscopy (TEM) were used to characterize the morphology and the size of the as-synthesized samples. A Philips X-ray diffractometer and energy-dispersive X-ray spectroscopy (EDS) were used to investigate the chemical composition. The structure detail of the manganites was characterized using a Hitachi HF-2000 high-resolution transmission electron microscope (FEG). We used an Axiovert S100 (Zeiss) fluorescent microscope, equipped with a 100 W mercury lamp. The photoluminescence is measured by a SPEX Fluorolog-2 spectrofluorometer.

3. Results and Discussion

The morphology and the chemical composition of the as-synthesized samples are characterized in Figure 1. A SEM image of the $BaMnO_3$ sample at 170 °C for 72 h is shown in Figure 1a, exhibiting nanorods with a thickness of 20−30 nm, width of 50−100 nm, and length of 600−1000 nm. The X-ray diffraction (XRD) pattern in Figure 1b shows that the product is hexagonal $BaMnO_3$ with lattice constants of $a = 5.699$ Å and $c = 4.817$ Å (JCPDS-260168, $P6_3/mmc$ (194)). When 50% of atoms at the Mn sites in barium manganite are substituted by Ti, $BaTi_{0.5}Mn_{0.5}O_3$ is received. A SEM image of the $BaTi_{0.5}Mn_{0.5}O_3$ at 200 °C for 48 h is shown in Figure 1c, displaying the products are elliptical nanorods 20−50 nm in width, 20 nm in thickness, and 100−500 nm in length. XRD measurement shows that the crystalline structure of the material is the same as $BaMnO_3$ in Figure 1d, but the counterpart peaks are negatively shifted due to the fact that the effective ionic radius of Ti (60.5 pm) is bigger than that of Mn (53 pm).[31] The crystal planes become bigger when Ti with a bigger effective ionic radii is substituted for Mn.

The TEM images in Figure 2 further investigate the details of $BaMnO_3$ at 200 °C for 120 h. The morphology of $BaMnO_3$ is clearly shown in Figure 2a. EDS proved that there are only three types of elements, Ba, Mn, and O, in the sample, as shown in Figure 2b. The Si signal came from the TEM grid. The electronic diffraction pattern of a single nanorod and high-resolution transmission electron microscopy (HRTEM) (Figure 2c−e) show that the nanorods are single crystals with the flat plane of (100) and the growth direction of [001].

Figure 3a shows that the morphology of $BaTi_{0.5}Mn_{0.5}O_3$ synthesized at 200 °C for 48 h is different from that of $BaMnO_3$ and $BaTiO_3$ (ref 30). EDS shows the atomic ratio of Mn to Ti is close to 1.0 in Figure 3b. The electronic diffraction pattern of a single nanorod and HRTEM show that each nanorod is a single crystal (Figure 2c−e) with the flat plane of (010) and the growth direction of [101].

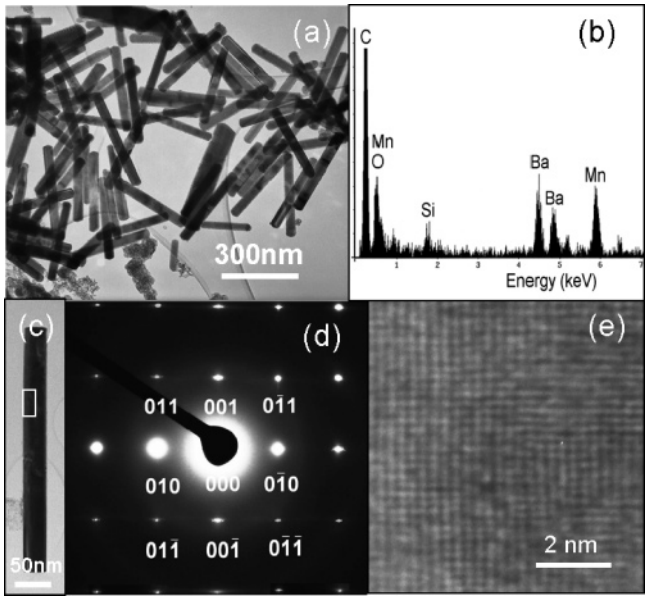

Figure 2. TEM images of $BaMnO_3$ at 200 °C for 120 h. (a) TEM image and (b) EDS spectrum showing the presence of Ba, Mn, and O. The Si signal came from the TEM grid. (c) An elected nanorod and its (d) diffraction pattern and (e) HRTEM image showing a single crystal with the growth direction of [001].

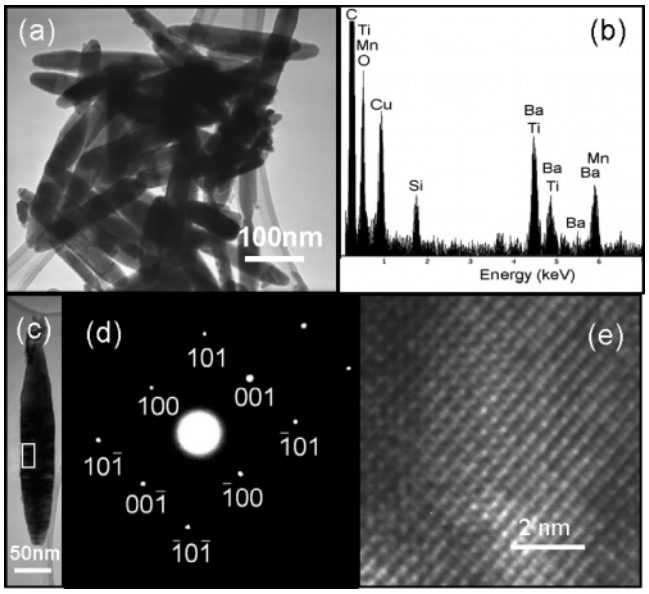

Figure 3. TEM images of the $BaTi_{0.5}Mn_{0.5}O_3$ nanorods at 200 °C for 48 h: (a) TEM image of the $BaTi_{0.5}Mn_{0.5}O_3$ nanorods; (b) EDS showing the presence of Ba, Ti, Mn, and O; (c) a single nanostructure and (d) its electron diffraction pattern as well as its (e) HRTEM image showing a single crystal with the growth direction of [101].

The shape and length of $BaMnO_3$ nanorods can be easily adjusted by varying the reaction conditions, such as heating temperature and/or heating time, during the synthesis process, as is shown in Figure 4. The nanorods have a width of 30 nm and a length of less than 100 nm when we synthesize them at 200 °C for 24 h (Figure 4a). However, the length can be greatly increased when we prolong the growth time under the same temperature, as is shown in Figure 4b, exhibiting a length of 200−400 nm for 120 h of growth. However, both the length and width can be enlarged when the growth temperature is lowered, and the width and length can reach 50−100 and 600−1000 nm, respectively, at 170 °C for 72 h (Figure 4c). More interesting, the shape can be changed when we add 1 mL of

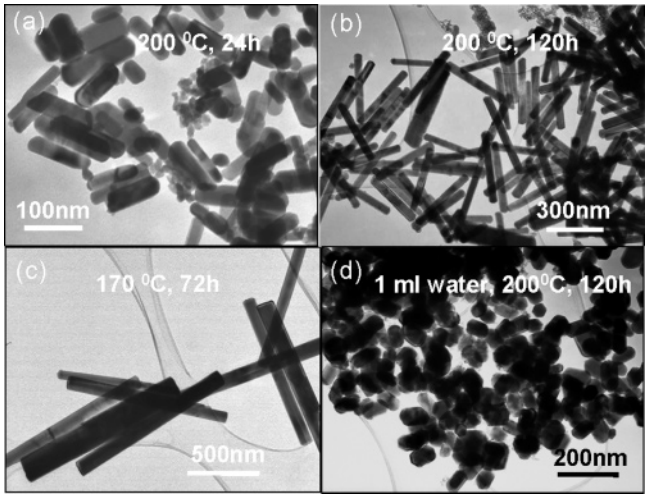

Figure 4. TEM images of $BaMnO_3$ grown at different times and temperatures: (a) at 200 °C for 24 h; (b) at 200 °C for 120 h; (c) at 170 °C for 72 h; (d) at 200 °C for 120 h, adding 1 mL of water.

water at a temperature of 200 °C for 120 h of growth, displaying the particle shape with a diameter of 50 nm. It demonstrates that the composite-hydroxide-mediated route is more suitable to one-dimensional nanostructure than hydrothermal synthesis.

From the above experimental results, a possible reaction mechanism for the synthesis of $BaMnO_3$ and $BaTi_{0.5}Mn_{0.5}O_3$ in hydroxide solution is suggested as the following. Although the molting points of both pure sodium hydroxide and potassium hydroxide are over 300 °C, $T_m = 323$ °C for NaOH and $T_m = 360$ °C for KOH, the eutectic point at NaOH/KOH = 51.5:48.5 is only about 165 °C (see ref 30). This is likely the key for synthesizing the manganites at ∼200 °C or lower. During the reaction process, hydroxides play a role not only as a solvent but also as a reactant for decreasing the reaction temperature. In the molten hydroxide, MnO_2 reacts with NaOH/KOH and forms hydroxide-soluble Na_2MnO_3/K_2MnO_3. To simplify the expression for chemical reactions here, we only include NaOH in the formula for simplicity.

The mechanism about the formation of $BaMnO_3$ is described as the following:

$$BaCl_2 + NaOH \rightarrow Ba(OH)_2 + 2NaCl \quad (7)$$

$$MnO_2 + 2NaOH \rightarrow Na_2MnO_3 + H_2O \quad (8)$$

and

$$Ba(OH)_2 + Na_2MnO_3 \rightarrow BaMnO_3 + 2NaOH \quad (9)$$

For $Ba(Ti_xMn_{1-x})O_3$,

$$xTiO_2 + (1-x)MnO_2 + 2NaOH \rightarrow Na_2(Ti_xMn_{1-x})O_3 + H_2O \quad (10)$$

and

$$Ba(OH)_2 + Na_2(Ti_xMn_{1-x})O_3 \rightarrow Ba(Ti_xMn_{1-x})O_3 + 2NaOH \quad (11)$$

Because the viscosity of hydroxide is large, the formation of $BaMnO_3$ and $BaTi_{0.5}Mn_{0.5}O_3$ nanostructures is slow and it is not easy for the nanostructures to agglomerate. This is likely the key for receiving dispersive single-crystalline nanostructures during the reaction without using a surface capping material.

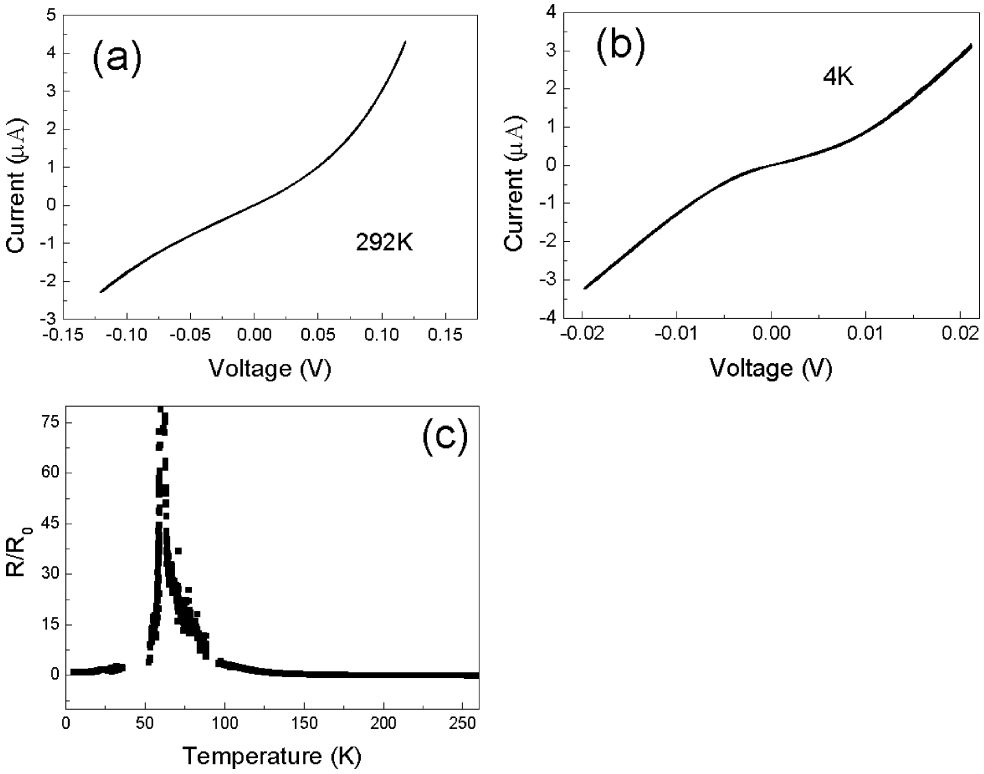

Figure 5. $I-V$ curves (a) at room temperature and (b) 4 K and a relative resistance versus temperature plot (c) for the sample of $BaMnO_3$ nanorods grown at 200 °C for 120 h.

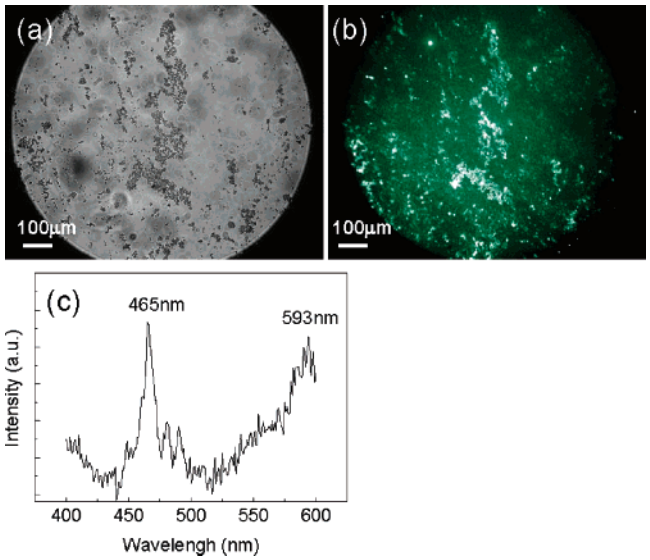

Figure 6. (a) Magnified bright and (b) fluorescence images as well as (c) the photoluminescence spectrum under an excitation wavelength of 350 nm for the $BaTi_{0.5}Mn_{0.5}O_3$ nanorods grown at 200 °C for 48 h.

The hydroxides mediate the reaction, but they are not part of the final nanostructures.

To investigate the electrical properties of $BaMnO_3$ nanorods, we built the film by dispersing $BaMnO_3$ nanorods in ethanol and casting it onto the Si wafer. $I-V$ and relative resistance versus temperature measurement has been carried out for the sample grown at 200 °C for 120 h. Figure 5 shows $I-V$ curves of the $BaMnO_3$ sample at room temperature (a) and 4 K (b).There are small differences for the $BaMnO_3$ sample at room temperature and 4 K, indicating the phases of $BaMnO_3$ at 4 K ($P6_3cm$; $a = 9.8467$, $c = 4.8075$) are different from those at room temperature ($P6_3/mmc$; $a = 5.6991$, $c = 4.1848$).[32] A relative resistance versus temperature plot from 4 to 250 K for the $BaMnO_3$ sample is given in Figure 5c. The big peak can be seen at 58 K from the plot, which indicates the phase transition happened at this temperature.[32]

It is known that $BaTi_{0.5}Mn_{0.5}O_3$ is a high dielectric material[33] and $BaMnO_3$ is not a luminescent material. However, our photoluminescent experiment demonstrates that when half of the atoms at the Mn sites in $BaMnO_3$ are substituted by the transition metal Ti, $BaTi_{0.5}Mn_{0.5}O_3$ nanorods can possess a very good photoluminescent property. Figure 6 shows 40 magnified bright (a) and fluorescence (b) images of $BaTi_{0.5}Mn_{0.5}O_3$ nanorods, exhibiting clearly green fluorescence from $BaTi_{0.5}Mn_{0.5}O_3$ nanorods. To further understand the fluorescence property, we measured the photoluminescence spectrum in Figure 6c under an excitation wavelength of 350 nm. There are two emission wavelengths from the photoluminescence spectrum: one is around 465 nm, and the other is around 593 nm. The green fluorescence in Figure 5b comes from an emission wavelength of 593 nm in the photoluminescence spectrum.

4. Conclusions

Single-crystalline nanorods of barium manganite ($BaMnO_3$) and barium titanium manganite ($BaTi_{1/2}Mn_{1/2}O_3$) have been successfully synthesized by using the composite-hydroxide-mediated approach. The size and shape can be easily manipulated by adjusting the growth time and temperature or adding a small amount of water in the process of synthesis. This is very important for detailed investigations of size effects on nanomanganites and realization of nanodevices. Resistance measurement shows that a phase transition happened at 58 K on $BaMnO_3$. The photoluminescence spectrum of $BaTi_{1/2}Mn_{1/2}O_3$ presents two emission peaks at wavelengths of 465 and 593 nm, corresponding to blue and green fluorescence.

Acknowledgment. This work is funded by NSFC (nos. 60376032, 90406024, 50572052), NSF, DARPA, and CCNE from NIH.

References and Notes

(1) Wang, Z. L. *Nanowires and nanobelts*; Kluwer Academic Publishers: Boston, MA, 2003.
(2) Wang, Z. L. *Mater. Today* **2004**, June, 26−33.
(3) Alivisatos, A. P. *Science* **1996**, *271*, 933.
(4) Fath, M.; Freisem, S.; Menovsky, A. A.; Tomioka, Y.; Aarts, J.; Mydosh, J. A. *Science* **1999**, *285*, 1540.
(5) Renner, C.; Aeppli, G.; Kim, B.-G.; Soh, Y.-A.; Cheong, S.-W. *Nature* **2002**, *416*, 518.
(6) Loudon, J. C.; Mathur, N. D.; Midgley, P. A. *Nature* **2002**, *420*, 797.
(7) Sun, J. Z.; Abraham, D. W.; Rao, R. A.; Eom, C. B. *Appl. Phys. Lett.* **1999**, *74*, 3017.
(8) Zhang, J.; Tanaka, H.; Kanki, T.; Choi, J.-H, Kawai, T. *Phys. Rev. B* **2001**, *64*, 184404.
(9) Park, J.-H.; Vescovo, E.; Kim, H.-J.; Kwon, C.; Ramesh, R.; Venkatesan, T. *Phys. Rev. Lett.* **1998**, *81*, 1953.
(10) Calderon, M. J.; Brey, L.; Guinea, F. *Phys. Rev. B* **1999**, *60*, 6698.
(11) Solovyev, I. V.; Terakura, K. *Phys. Rev. B* **2001**, *63*, 174425.
(12) Kong, X. Y.; Ding, Y.; Yang, R. S.; Wang, Z. L. *Science* **2004**, *303*, 1348.
(13) Yang, P.; Deng, T.; Zhao, D.; Feng, P.; Pine, D.; Chmelka, B. F.; Whitesides, G. M.; Stucky, G. D. *Science* **1998**, *282*, 2244.
(14) Wang, X.; Zhuang, J.; Peng, Q.; Li, Y. *Nature* **2005**, *437*, 121.
(15) O'Brien, S.; Brus, L.; Murray, C. B. *J. Am. Chem. Soc.* **2001**, *123*, 12085.
(16) Urban, J. J.; Yun, W. S.; Gu, Q.; Park, H. *J. Am. Chem. Soc*. **2002**, *124*, 1186.
(17) Zhu, D.; Zhu, H.; Zhang, Y. *Appl. Phys. Lett.* **2002**, *80*, 1634.
(18) Spooren, J.; Rumpecker, A.; Millange, F.; Walton, R. I. *Chem. Mater.* **2003**, *15*, 1401.
(19) Mao, Y. B.; Banerjee, S.; Wong, S. S. *Chem. Commun.* **2003**, 408.
(20) Liu, J.; Wang, H.; Zhu, M.; Wang, B.; Yan, H. *Mater. Res. Bull*. **2003**, *38*, 817.
(21) Budhani, R. C.; Roy, C.; Lewis, L. H.; Li, Q.; Moodenbaugh, A. R. *J. Appl. Phys.* **2000**, *87*, 2490.
(22) Bilger, S.; Syskakis, E.; Naoumidia, A.; Nickel, H. *J. Am. Ceram. Soc.* **1992**, *75*, 964.
(23) Vázquez-Vázquez, C.; Blanco, M. C.; López-Quintela, M. A.; Sánchez, R. D.; Rivas, J.; Oseroff, S. B. *J. Mater. Chem.* **1998**, *8*, 991.
(24) Philip, J.; Kutty, T. R. N. *Mater. Chem. Phys.* **2000**, *63*, 218.
(25) Ramanathan, S.; Singh, P. K.; Kakade, M. B.; De, P. K. *J. Mater. Sci*. **2004**, *39*, 3207.
(26) Spooren, J.; Walton, R. I.; Millange, F. *J. Mater. Chem.* **2005**, *15*, 1542.
(27) Urban, J. J.; Ouyang, L.; Jo, M.-H.; Wang, D. S.; Park, H. *Nano Lett.* **2004**, *4*, 1547.
(28) Zhu, D.; Zhu, H.; Zhang, Y. *Appl. Phys. Lett.* **2002**, *80*, 1634.
(29) Zhang, T.; Jin, C. G.; Qian, T. X.; Lu, L.; Bai, J. M.; Li, X. G. *J. Mater. Chem.* **2004**, *14*, 2787.
(30) Liu, H.; Hu, C. G.; Wang, Z. L. *Nano. Lett.*, in press.
(31) Dean, J. A. *Lange's Handbook of Chemistry*; McGraw-Hill: New York, 1999.
(32) Cussen, E. J.; Battle, P. D. *Chem. Mater*. **2000**, *12*, 831.
(33) Keith, G. M.; Sarma, K.; Alford, N. M.; Cussen, E. J.; Rosseinsky, M. J. Sinclair, D. C. *Chem. Mater.* **2004**, *16*, 2007.